Kinetic analysis of active omni wheel with barrel-shaped rollers for avoiding slippage and vibration

Siying Long
Department of Mechanical Engineering and Science, Kyoto University
Kyoto daigaku-katsura, Nishikyo-ku, Kyoto, 615-8540, Japan
E-mail: long.siying.o97@kyoto-u.jp

Tatsuro Terakawa[1]
Department of Mechanical Engineering and Science, Kyoto University
Kyoto daigaku-katsura, Nishikyo-ku, Kyoto, 615-8540, Japan
E-mail: terakawa@me.kyoto-u.ac.jp

Mahiro Yogou
Department of Mechanical Engineering and Science, Kyoto University
Kyoto daigaku-katsura, Nishikyo-ku, Kyoto, 615-8540, Japan
E-mail: mahiro.g.rx0@gmail.com

Rintaro Koyano
Department of Mechanical Engineering and Science, Kyoto University
Kyoto daigaku-katsura, Nishikyo-ku, Kyoto, 615-8540, Japan
E-mail: koyano.rintaro.38s@gmail.com

Masaharu Komori
Department of Mechanical Engineering and Science, Kyoto University
Kyoto daigaku-katsura, Nishikyo-ku, Kyoto, 615-8540, Japan
E-mail: komorim@me.kyoto-u.ac.jp

ABSTRACT

Omnidirectional mobility is required for the efficient movement of transport vehicles in factories and warehouses. To meet this requirement, the active omni wheel with barrel-shaped rollers (AOWBR) was previously proposed. The barrel-shaped rollers are arranged around the outer circumference of the main wheel of the AOWBR. This structure is expected to be effective in suppressing vibration during vehicle movement. The transmission roller drives the outer roller via a friction drive, which actively moves the AOWBR in the lateral direction. However, the friction drive may cause slippage between the transmission roller and the outer roller. To solve this problem, this study investigates the effects of the design parameters for an AOWBR on vibration and wheel slippage. The kinetic models of the wheel main body, transmission roller, and outer roller are established. Then, simulations are carried out using the kinetic models for various structural parameter values. The simulation results show that a softer rubber block installed in the support mechanism of the outer roller contributes to reduce wheel slippage but cause larger vibration, and that a larger setting angle between the transmission and outer rollers contributes to

[1] Corresponding author.

reduce slippage and vibration. Finally, comparison experiments are conducted on two types of prototype to verify the simulation results.

Keywords: Omnidirectional mobility, Active omni wheel, Mechanism design, Kinetics, Slippage, Vibration

1. INTRODUCTION

Transport vehicles are widely used to deliver materials in warehouses and factories. To improve their maneuverability and usability, various omnidirectional wheel mechanisms that allow immediate movement in an arbitrary direction have been proposed [1-4]. The omni wheel has several free rollers arranged around its outer circumference [5-10]. These rollers can rotate passively, which enables the lateral movement of the omni wheel. The Mecanum wheel has several passive rollers arranged across its periphery at a specific angle [11-16]. A vehicle equipped with Mecanum wheels can realize omnidirectional mobility similar to that realized with omni wheels. The spherical wheel is driven by rollers and can move in an arbitrary direction [17-22]. The above mechanisms have some limitations. It is difficult to precisely control the movement of the omni wheel and the Mecanum wheel because of the rotational resistance of the free rollers. Additionally, more than two wheels are necessary for movement in an arbitrary direction. Although a vehicle equipped with a single spherical wheel can move in any direction, the volume of the spherical wheel is large and self-balancing control must be developed.

To overcome these limitations, the authors previously proposed the active omni wheel (AOW) [23-25]. The AOW has a disk-shaped main wheel, and multiple outer rollers are attached around the outer circumference of this wheel. The rotations of two motors are successively transmitted to the main wheel and outer rollers through the

differential gear mechanism. Therefore, the AOW can be made to move in an arbitrary direction by controlling the rotational velocities of the motors. However, the AOW provides poor ride comfort because of the vertical vibration during movement caused by the gaps between the outer rollers.

To solve this problem, an active omni wheel with barrel-shaped rollers (AOWBR), shown in Fig. 1, was proposed [26, 27]. The barrel-shaped rollers are arranged alternately around the outer circumference of the main wheel. This roller structure eliminates the gaps between the outer rollers and thus effectively reduces the vertical vibration. When input shaft 1 is rotated at the same velocity as that of input shaft 2, the main wheel rotates around the wheel axle. As a result, the AOWR moves in the wheel plane direction. When the rotational velocities of input shafts 1 and 2 are equal but opposite, the rotation of the input shafts is transmitted to the transmission rollers. Then, the outer rollers are driven through friction. As a result, the AOWR moves in the direction vertical to the wheel plane. When the rotational velocities of input shafts 1 and 2 are different, the two motions described above occur simultaneously. As a result, the AOWR moves in a diagonal direction. The friction drive between a transmission roller and an outer roller simplifies the drive system and reduces the number of parts that comprise the wheel mechanism.

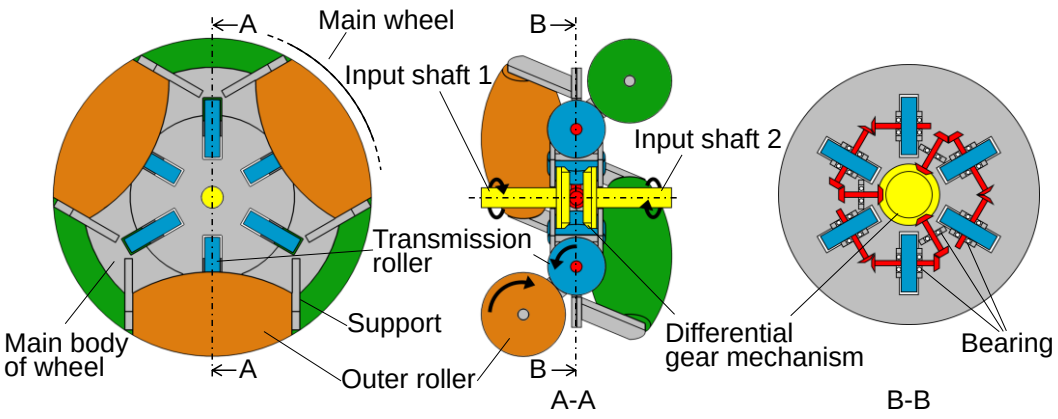

Fig. 1 Structure of AOWBR with six outer rollers [26].

In the previous study [26], the kinematics of the AOWBR was analyzed and its fundamental effectiveness was confirmed through experiments. However, several issues emerged from the result. There is a concern regarding slippage between the transmission and outer rollers, which leads to a loss of the traveling performance of the vehicle equipped with the AOWBR. Another common problem for omnidirectional wheel mechanism is the vibration during traveling [28, 29]. The vibration suppression effect of the AOWBR was demonstrated for a single design, but its theoretical substantiation nor effectiveness in a general context have not been demonstrated. To solve the above problem, this study investigates the relationship between the dynamic behavior (e.g., slippage and vibration) and the structural parameters of the AOWBR. Then, the appropriate conditions for a practical design are identified. First, kinetic models of the wheel main body, outer roller, and transmission roller are constructed based on the Newton-Euler equation. Simulations are then conducted using the kinetic models. The variation of the dynamic characteristics of the AOWBR is analyzed and

discussed based on the simulation results. Finally, experiments are conducted on two types of prototype vehicle to verify the simulation results.

2. KINETIC MODEL FOR ACTIVE OMNI WHEEL WITH BARREL-SHAPED ROLLERS

The kinetic model for the AOWBR is established in this section. To clarify the dynamic behavior of the AOWBR when the ground contact point changes, this study investigates forward motion. Considering the structural symmetry of the mechanism, we focus on the period during which one of the outer rollers contacts the ground. It is assumed that there is no slip between the ground and the wheel.

As explained in the previous section, the AOWBR is composed of the wheel main body, transmission rollers, and outer rollers. Each outer roller is supported by a holding mechanism at each end. The holding mechanisms are fixed to the wheel main body. As shown in Fig. 2, a rubber block is placed between the outer roller axle and a holding mechanism so that an outer roller can keep in contact with its corresponding transmission roller while it is in contact with the ground. The transmission rollers are rotationally supported by the wheel main body. The kinetic model for the AOWBR is separated into those of the wheel main body, transmission roller, and outer roller, as described in the following sections.

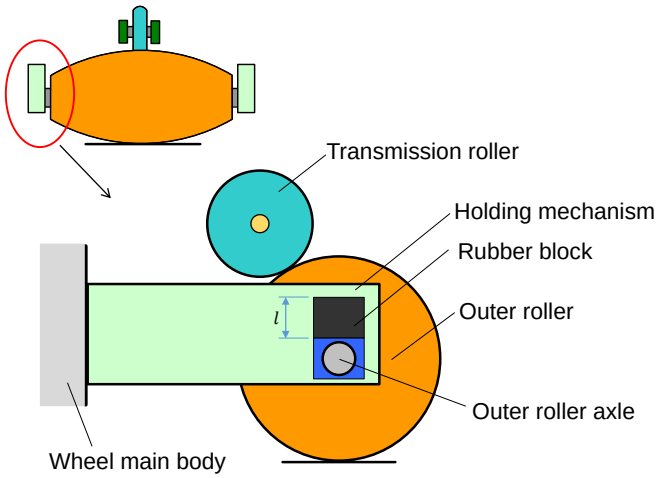

Fig. 2 Holding mechanism of outer roller.

To construct the kinetic model for the AOWBR, three right-hand orthogonal coordinate systems are established, as shown in Fig. 3. The coordinate systems Σ_{G1}, Σ_{G2}, and Σ_{G3} are set with their origins at the center point of the wheel main body G_1, the center point of the transmission roller G_2, and the center point of the outer roller G_3, respectively. All X_i axes of the coordinate systems are normal to the paper surface. The Y_1-axis is parallel to the ground, the Y_2-axis is parallel to the roller axle of the transmission roller, and the Y_3-axis is parallel to the roller axle of the outer roller.

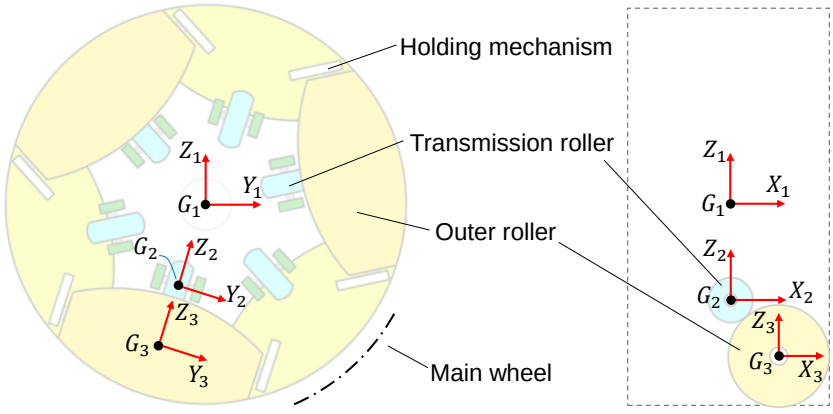

Fig. 3 Coordinate systems used for modeling.

2.1 Kinetic model for wheel main body

The force from the transmission roller and the outer roller to the wheel main body is shown in Fig. 4. The forces from the transmission roller at each end along the positive X_2-, Y_2-, and Z_2-axes are F_{2ax}, F_{2bx}, F_{2ay}, F_{2by}, F_{2az}, and F_{2bz}, respectively. Similarly, the forces from the outer roller at each end along the positive X_3-, Y_3-, and Z_3-axes are F_{3ax}, F_{3bx}, F_{3ay}, F_{3by}, F_{3az}, and F_{3bz}, respectively. Therefore, the kinetic model for the wheel main body is written as:

$$\begin{cases} m_1\ddot{x}_1 = F_{2ax} + F_{2bx} + F_{3ax} + F_{3bx} \\ m_1\ddot{y}_1 = (F_{2az} + F_{2bz} + F_{3az} + F_{3bz})\sin\theta_1 + \left(F_{2ay} + F_{2by} + F_{3ay} + F_{3by}\right)\cos\theta_1 - C_{rr}N \\ m_1\ddot{z}_1 = (F_{2az} + F_{2bz} + F_{3az} + F_{3bz})\cos\theta_1 \ - \left(F_{2ay} + F_{2by} + F_{3ay} + F_{3by}\right)\sin\theta_1 - m_1 g \\ I\ddot{\theta}_1 = \tau_1 + (F_{2bz} - F_{2az})L_2 + (F_{3bz} - F_{3az})L_3 + \left(F_{2ay} + F_{2by}\right)l_2 \cdots \\ +(R_0 - r_{max} - z_3)\left(F_{3ay} + F_{3by}\right) \\ l_2 = R_0 - (1 + \sin\gamma)r_{max} - r_d\sin\gamma \end{cases} , \quad (1)$$

where m_1 is the mass of the wheel main body, N is the normal force from the wheel to the ground, C_{rr} is the resistance coefficient, g is the gravitational acceleration, l_2 is the distance from the center point of the wheel main body to that of the transmission roller, L_2 is the distance from the center point of the transmission roller to its support point, L_3 is the distance from the center point of the outer roller to the holding mechanism, I is the inertia moment of the wheel main body around the X_1-axis, θ_1 is the rotation angle of the wheel main body around the X_1-axis, τ_1 is the driving torque carried on the wheel main body, R_0 is the radius of the main wheel without consideration of the deformation of the outer roller, r_{max} is the maximum radius of the cross section of the outer roller,

r_d is the radius of the transmission roller, and z_3 is the deformation of the outer roller along the Z_3-axis.

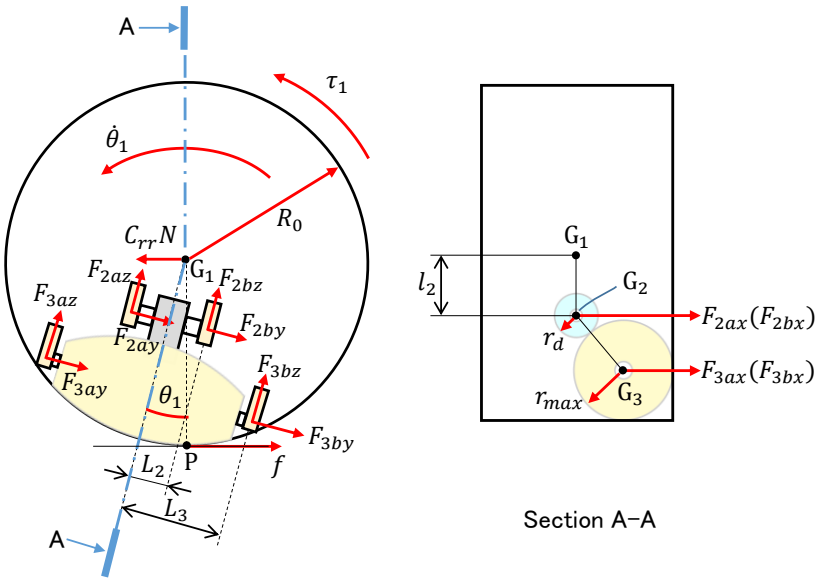

Fig. 4 Force model for wheel main body.

2.2 Kinetic model for transmission roller

The force applied on the transmission roller is shown in Fig. 5. The transmission roller cannot revolve around the X_2- and Z_2- axes because it is fixed to the wheel main body. Therefore, with consideration of the external force and the apparent force, the Newton-Euler motion equations for the transmission roller are written as:

$$\begin{cases} m_2\ddot{x}_2 = -N_d\cos\gamma - F_{2ax} - F_{2bx} \\ m_2\ddot{y}_2 = (m_2 g + m_2\ddot{z}_1)\sin\theta_1 - m_2\ddot{y}_1\cos\theta_1 + m_2 l_2\ddot{\theta}_1 - F_{2ay} - F_{2by} \\ m_2\ddot{z}_2 = -(m_2 g + m_2\ddot{z}_1)\cos\theta_1 - m_2\ddot{y}_1\sin\theta_1 - m_2 l_2\dot{\theta}_1^2 + N_d\sin\gamma - F_{2az} - F_{2bz} \\ L_2F_{2az} - L_2F_{2bz} = 0 \\ L_2F_{2bx} - L_2F_{2ax} = 0 \end{cases}, \quad (2)$$

where m_2 is the mass of the transmission roller, N_d is the pressing force from the outer roller to the transmission roller, and γ is the setting angle between the transmission roller and the outer roller.

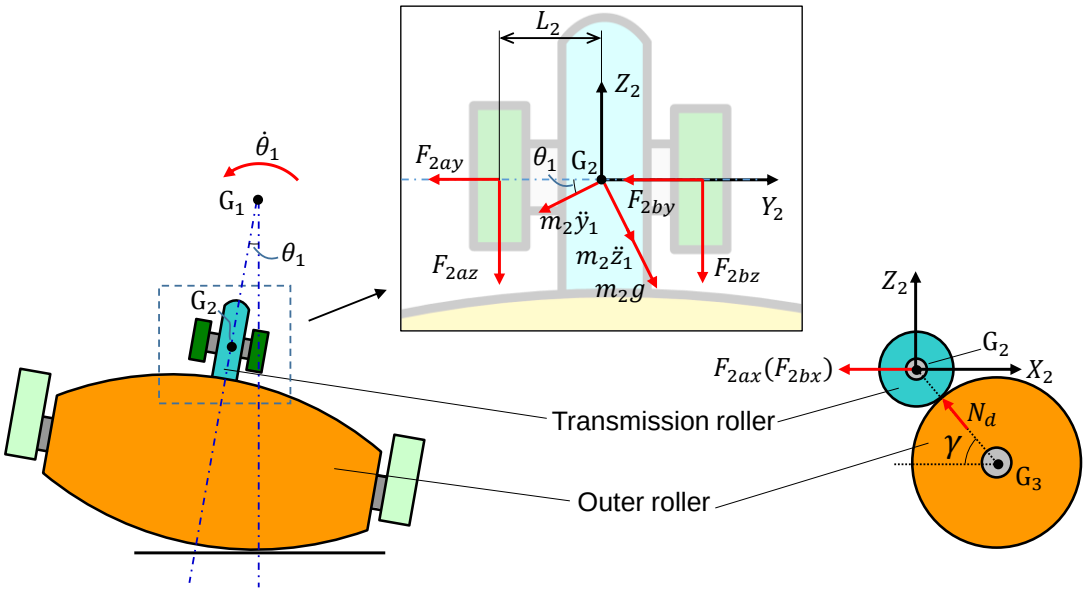

Fig. 5 Force model for transmission roller.

2.3 Kinetic model for outer roller

The force model corresponding to the outer roller is shown in Fig. 6. Similar to the kinetic model for the transmission roller, that for the outer roller is written as:

$$\begin{cases} m_3\ddot{x}_3 = N_d\cos\gamma - F_{3ax} - F_{3bx} \\ m_3\ddot{y}_3 = (m_3g + m_3\ddot{z}_1)\sin(\theta_1-\theta_3) - m_3\ddot{y}_1\cos(\theta_1-\theta_3)\cdots \\ +m_3\left[(R_0 - r_{max} - z_3)\ddot{\theta}_1 - 2\dot{z}_3\dot{\theta}_1\right] + f\cos(\theta_1-\theta_3) - N\sin(\theta_1-\theta_3) - F_{3ay} - F_{3by} \\ m_3\ddot{z}_3 = -(m_3g + m_3\ddot{z}_1)\cos(\theta_1-\theta_3) - m_3\ddot{y}_1\sin(\theta_1-\theta_3)\cdots \\ -m_3(R_0 - r_{max} - z_3)\dot{\theta}_1^2 - N_d\sin\gamma + f\sin(\theta_1-\theta_3) + N\cos(\theta_1-\theta_3) - F_{3az} - F_{3bz} \\ I_3\ddot{\theta}_3 = L_3F_{3az} - L_3F_{3bz} + [(R_0 - r_{max} - z_3)(\sin\theta_1 - \sin(\theta_1-\theta_3)) - z_3\sin\theta_1]N \end{cases}, \tag{3}$$

where m_3 is the mass of the outer roller, I_3 is the inertia moment of the outer roller around the X_3-axis, θ_3 is the rotation angle of the outer roller around the X_3-axis, and f is the driving force.

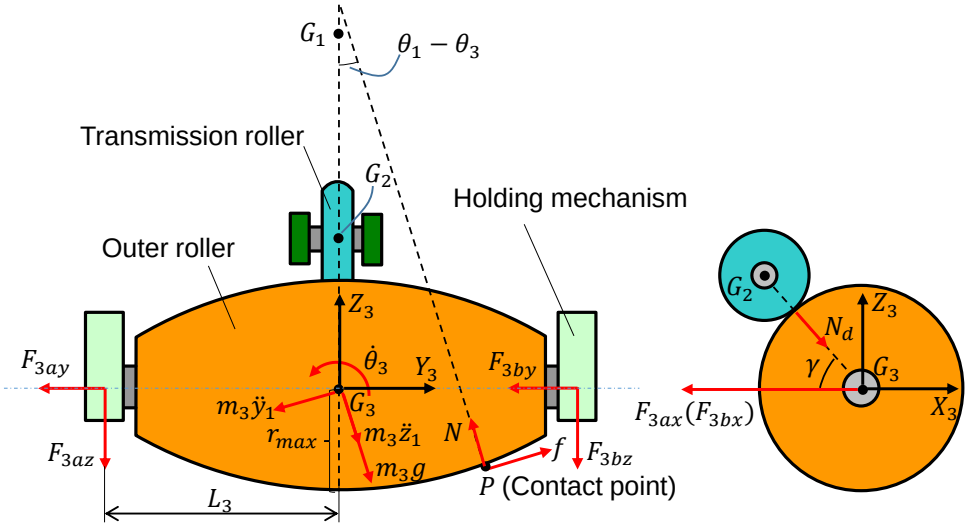

Fig. 6 Force model for outer roller.

The displacement of the outer roller along the Z_3-axis direction z_3 causes a vertical displacement of the wheel main body by $z_3 \cos\theta_1$. Additionally, the rotation of the outer roller around the X_3-axis makes an eccentric circular motion of the circumference of the wheel main body as shown in Fig. 7. Therefore, the relationship between z_1 and z_3 is written as:

$$z_1 = z_3 \cos\theta_1 + (R_0 - r_{max} - z_3)\{\cos(\theta_1 - \theta_3) - \cos\theta_1\}. \quad (4)$$

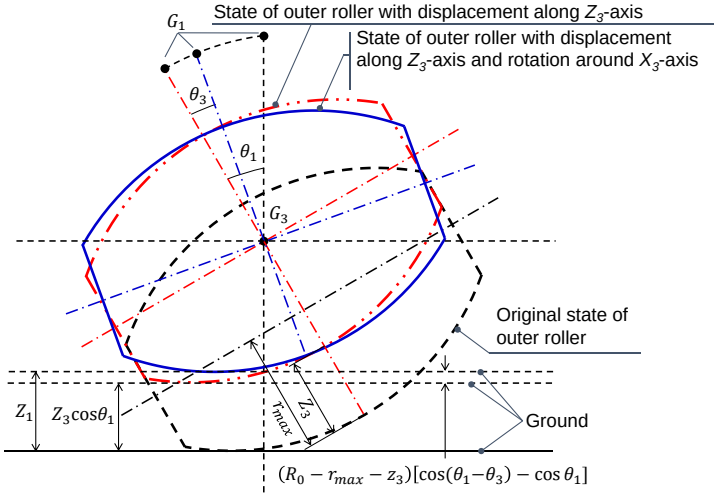

Fig. 7 Deformation of main wheel considering eccentric circular motion of outer roller.

2.4 Elastic force acting on outer roller

The pressing between the transmission roller and the outer roller occurs via rubber blocks. The rubber block between the outer roller axle and the holding mechanism shown in Fig. 2 is deformed when the outer roller is in contact with the ground. This generates elastic forces, which are modeled in this section. Considering the elasticity of the roller surfaces and rubber blocks, it is assumed that the transmission roller, outer roller, and holding mechanism constitute an elastic system, as shown in Fig. 8.

Given that the modulus of elasticity between the transmission roller and outer roller k_1 is constant since the deformation between them is considered to be limited, the pressing force is written as:

$$N_d = k_1 z_3 \sin\gamma. \tag{5}$$

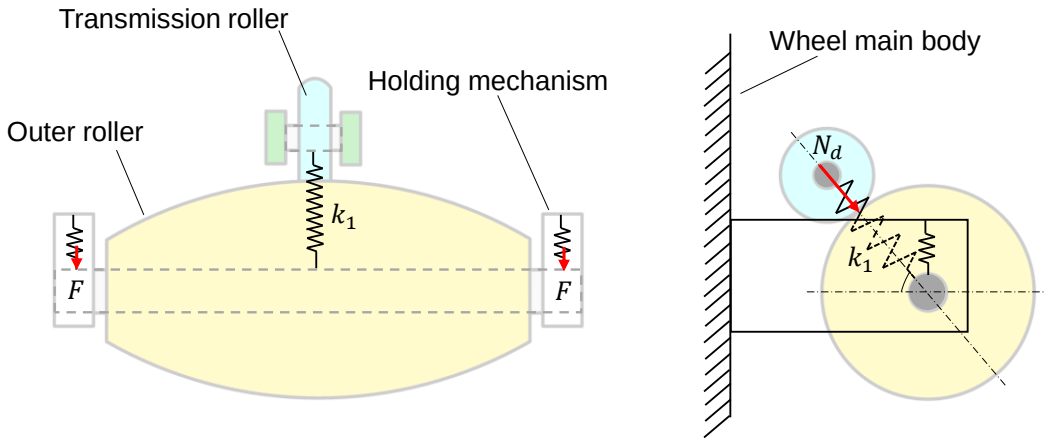

Fig. 8 Elastic system constructed by transmission roller, holding mechanisms, and outer roller.

According to studies on the deformation of rubber [30, 31], the stress F generated by the rubber block can be calculated as:

$$F(\alpha) = K_t \left(\frac{\alpha_m}{2} \ln \frac{1+\alpha/\alpha_m}{1-\alpha/\alpha_m} - \frac{1}{\alpha^2} \right) + b, \tag{6}$$

where α is the elongation rate, K_t is a parameter that depends on the dicumyl peroxide content in the rubber, α_m is the maximum elongation rate for the rubber, and b is a correction term. Here, α_m also represents the hardness of the rubber, i.e., a larger α_m indicates a softer rubber.

In the AOWBR, the reaction force from the outer roller axle causes deformations of the rubber block installed in the holding mechanism. The elongation rate for the rubber blocks is calculated as:

$$\begin{cases} \alpha_l = 1 + \frac{|z_3 - L_3 \sin\theta_3|}{l} \\ \alpha_r = 1 + \frac{|z_3 + L_3 \sin\theta_3|}{l}, \end{cases} \tag{7}$$

where α_l and α_r are the elongation rates for the rubber block in the holding mechanism at the left and right sides, respectively, and l is the original length of the rubber block as shown in Fig. 2. Therefore, the stress generated by the rubber block can be calculated using Eqs. (6) and (7). The reaction force of the holding mechanism at the left and right sides, F_{3az} and F_{3bz}, respectively, is written as:

$$\begin{cases} F_{3az} = AF(\alpha_l) \\ F_{3bz} = AF(\alpha_r), \end{cases} \tag{8}$$

where A is the cross-sectional area of the rubber block.

3. MOTION SIMULATION

Based on the kinetic model constructed in the previous section, the dynamic characteristics of the AOWBR are analyzed through simulations. This study investigates the slip between rollers and vibration when the design parameters are varied. The

standard parameter values applied in the simulations are shown in Table 1. The mass and inertia moment are calculated under the assumption that the material of the wheel is S45C and the outer circumference of the outer roller is nylon. It is also assumed that the wheel is stationary in the initial state and that the driving torque τ_1 is constant. The rotation of the wheel main body is analyzed from $\theta_1 = -\pi/n$ to $\theta_1 = \pi/n$ with consideration of structural symmetry, where n is the number of outer rollers. The outer rollers are evenly distributed around the circumference of the main wheel. L_3 is thus determined using the equation $L_3 = R_0 \sin(\pi/n)$. The time interval in the simulation is set to 0.0001 s. The simulations are conducted in MATLAB R2020b running on a computer with an Intel Core i5-7500 CPU and 16 GB of RAM. The Runge-Kutta method was applied to solve the kinetic equations through the standard MATLAB toolbox. The velocity and acceleration in each direction are set to zero to obtain the initial solution.

The slippage and vertical vibration of the AOWBR are the main focus in this study. They are closely related to the pressing force between the transmission and outer rollers N_d and the vertical displacement of the wheel main body z_1. Therefore, they are analyzed when the following design parameters are varied: the hardness of the rubber block α_m, the setting angle of the outer roller γ, the maximum radius of the outer roller r_{max}, and the total number of outer rollers n.

Table 1 Standard parameter values used in simulation (parameters on left side were fixed and parameters on right side were varied)

Parameter	Value		Parameter	Value
m_2	0.12 kg		m_1	30.0 kg
R_0	150 mm		I	0.347 kg m^2
r_d	20 mm		m_3	3.3 kg
l	25 mm		I_3	4.43×10^{-2} kg m^2
τ_1	1 N m		γ	22°
C_{rr}	0.04		r_{max}	40 mm
k_1	297.39 N/mm		n	6
K_t	2.1		α_m	1.06
b	-1.8366 N/m^2			
A	60 mm^2			
g	9.8 m/s^2			

3.1 Simulation results for various values of hardness of rubber block

The variation of pressing force N_d and vertical displacement z_1 with maximum elongation rate α_m is shown in Fig. 9. Focusing on individual results, both N_d and z_1 oscillate as they change. This might be due to the elastic oscillation of the outer roller raised by the rubber block in the holding mechanism. Both curves have a roughly upward convex shape. The pressing force and displacement at around $\theta_1 = 0$, where the center of the outer roller contacts the ground, are larger than those at around $\theta_1 = \pm\pi/6$, where the end of the outer roller contacts the ground. The reason for this is considered to be as follows. The angle between the Z_3-axis and the direction of the reaction force from the ground becomes small because the ground contact point gets

close to the central plane of the outer roller. When the direction of the reaction force consists with the Z_3-axis, the maximum displacement of the outer roller is produced. The displacement decreases as the contact point leaves the central plane. This determines the behavior of z_1. The pressing force N_d shows a similar variation tendency because it depends on the displacement of the outer roller.

When the maximum elongation rate α_m is changed from 1.02 to 1.1, the pressing force N_d becomes larger along with the increment of α_m as shown in Fig. 9(a). This is because a softer rubber block in the holding mechanism increases the elastic deformation, and thus the displacement of outer roller becomes larger. For the same reason, the oscillation becomes stronger when α_m increases.

As shown in Fig. 9(b), the vertical displacement z_1 shows a tendency similar to that for the pressing force N_d shown in Fig. 9(a). Here, z_t is defined as the difference between the maximum and minimum displacement of z_1. The results show that both z_t and z_1 increase when the maximum elongation rate α_m increases. The oscillation of z_1 also becomes stronger when α_m increases. This may occur for the same reasons as those for the pressing force N_d mentioned above. The magnitudes of the oscillation and z_t are considered to reflect the amplitude of the vertical vibrations at different frequencies during travel along one outer roller section, and the magnitude of z_1 may be related to the vibration caused by the switching of the outer rollers. It is expected that a smaller α_m will lead to smaller vibration of the AOWBR.

In summary, when α_m is larger, both the pressing force N_d and vertical displacement z_1 become larger. This means that a softer rubber block in the holding mechanism

makes slippage between the transmission roller and the outer roller less likely to occur, but increases vibration. This tradeoff must be taken into account in the design of the AOWBR.

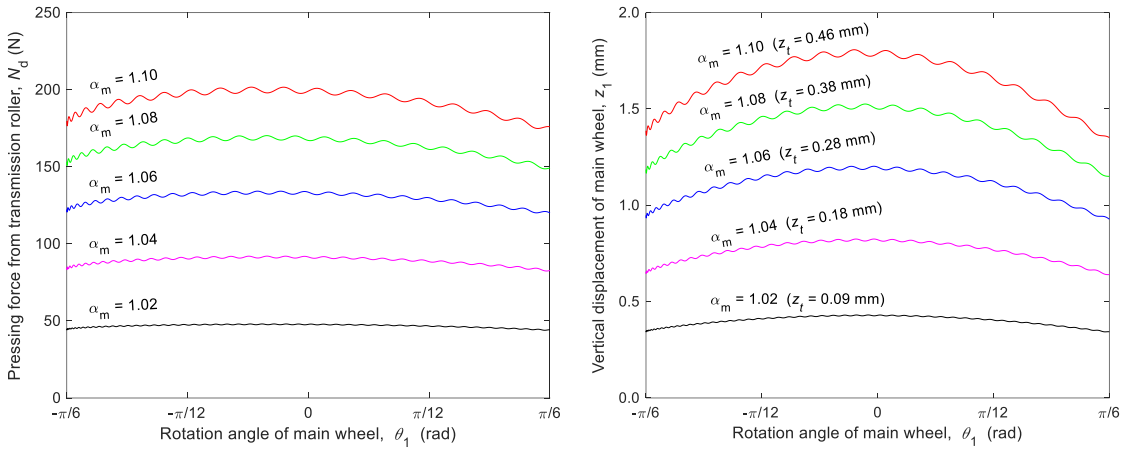

(a) (b)

Fig. 9 Variation of (a) pressing force N_d and (b) vertical displacement z_1 with maximum elongation rate of rubber block α_m.

3.2 Simulation results for various values of setting angle of outer roller

Next, the variation of the pressing force N_d and vertical displacement z_1 with the setting angle between the transmission roller and the outer roller γ is discussed. Here, the setting angle is set to $22°$, $45°$, $68°$, or $90°$. Note that $\gamma = 90°$ would cause interference between the outer rollers on the left and right sides in practice, but is allowed here for comparison. The other parameter values were those shown in Table 1. As shown in Fig. 10(a), the pressing force N_d is smallest for γ = $22°$. For setting angles of $45°$, $68°$, and $90°$, the pressing force is similar, with that for γ = $68°$ being slightly larger than the other two as shown in the enlarged view. This means that the pressing force N_d does not increase with the setting angle γ. In contrast, the vertical displacement z_1

decreases with the setting angle γ, as shown in Fig. 10(b). The maximum-minimum difference z_t and the oscillation strength only slightly change. The interaction between the pressing force N_d and the normal force from the ground becomes dominant in the force balance of the outer roller when the setting angle γ is increased. Therefore, the elastic forces of the holding mechanisms become relatively small, which leads to smaller displacements z_1 and z_3. The smaller displacement z_3 decreases the pressing force N_d. The contact between the transmission roller and the outer roller is assumed to be a spring, as shown in Fig. 8. The displacement direction of z_3 gradually becomes consistent with that of the equivalent spring when the setting angle γ is close to $90°$, which increases the pressing force N_d. Therefore, the pressing force N_d is considered to vary as shown in Fig. 10(a) because of the interaction between the above two factors.

In summary, a larger setting angle γ leads to a larger pressing force N_d and a smaller vertical displacement z_1. This means that a larger setting angle γ contributes to avoiding the slippage between the transmission roller and the outer roller and reducing vibration during movement. However, interference between the outer rollers may occur when the setting angle γ is larger than a certain value. Therefore, the setting angle γ should be set properly in the design with consideration of the interference between the outer rollers.

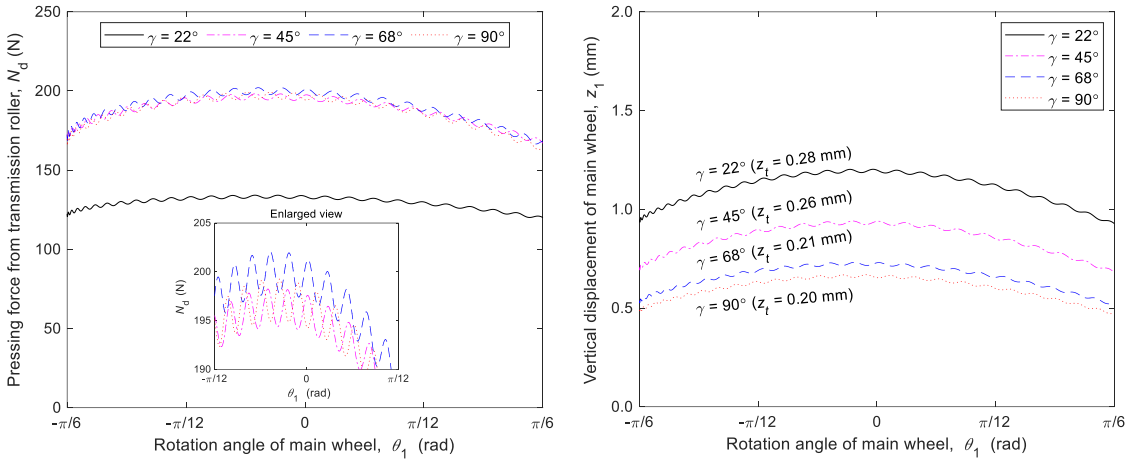

(a) (b)

Fig. 10 Variation of (a) pressing force N_d and (b) vertical displacement z_1 with setting angle of outer roller γ.

3.3 Simulation results for various values of radius of outer roller

Next, the variation of pressing force N_d and vertical displacement z_1 with the maximum radius of the cross section of the outer roller r_{max} is discussed. The simulation was conducted with $r_{max} = 30, 35, 40, 45,$ and 50 mm. The inertia parameters (e.g., m_3 and I_3) were recalculated from the values in Table 1 based on the assumption that the density of the outer roller is unchanged. The other parameter values were the same as those in Table 1. The simulation results are shown in Fig. 11. Both the pressing force N_d and vertical displacement z_1 are almost the same even when r_{max} is varied. We speculate that the pressing force N_d and vertical displacement z_1 are mainly affected by the elasticity of the holding mechanism and the transmission and outer rollers. Therefore, the variation of the radius and inertia of the outer roller hardly affects wheel slippage and vibration. Namely, the AOWBR has high design freedom in terms of r_{max} for avoiding wheel slippage and vibration.

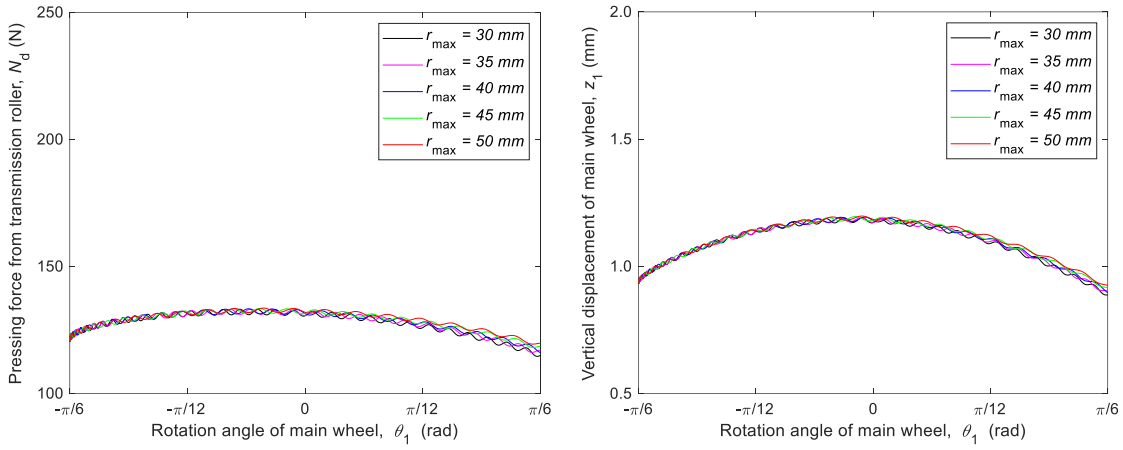

(a) (b)

Fig. 11 Variation of (a) pressing force N_d and (b) vertical displacement z_1 with maximum radius of outer roller r_{max}.

3.4 Simulation results for various numbers of outer rollers

Next, the variation of the pressing force N_d and vertical displacement z_1 with the total number of outer rollers n is discussed. The simulation was conducted with $n = 6$, 8, 10, and 12. The inertia parameters (e.g., m_3 and I_3) were calculated based on the assumption that the density of the outer roller is the same. The other parameter values were the same as those in Table 1. The variations of the pressing force N_d and vertical displacement z_1 are shown in Fig. 12. Both the pressing force N_d and vertical displacement z_1 increased slightly with the total number of outer rollers n. This shows that the total number of outer rollers n does not significantly affect the pressing force N_d and vertical displacement z_1. The elastic force of the holding mechanism is mainly affected by the elongation rate of the rubber block, which is determined by z_3, L_3, and θ_3 according to Eq. (7). Although the parameter L_3 decreases with the total number of outer rollers n, the elastic force of the holding mechanism only slightly changes because

θ_3 is relatively small. Therefore, the variation of these parameters only slightly affects the torque and force in the dynamic behavior of the AOWBR. The pressing force N_d and vertical displacement z_1 are thus not significantly affected by the total number of outer rollers n. This means that the total number of outer rollers n should not be a significant factor when considering wheel slippage and vibration in the design of the AOWBR.

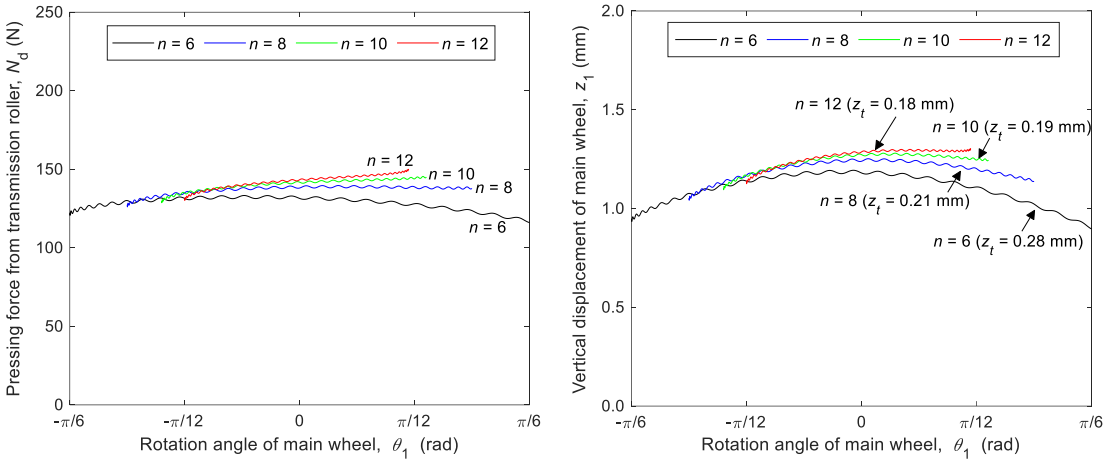

(a) (b)

Fig. 12 Variation of (a) pressing force N_d and (b) vertical displacement z_1 with total number of outer rollers n.

4. EXPERIMENT

To verify the simulation results, experiments were conducted on two types of prototype vehicle as described in this section. Based on the simulation results, the hardness of the rubber block in the holding mechanism, the setting angle between the transmission roller and the outer roller, and the total number of outer rollers were the main considerations in the development of the two types of prototype.

4.1 Experimental setup

Two types of prototype vehicle were developed for the experiments as shown in Fig. 13. Although the input shafts of the AOWBRs are placed on one side, the motion mechanism is the same as that of Fig. 1. Prototype A was developed in [26]. For this prototype, the vehicle is equipped with one AOWBR and a conventional omni wheel. Two rows of outer rollers (total of six rollers) are arranged around the circumference of the AOWBR. The setting angle between the transmission roller and the outer roller γ is $22°$. A rubber block is placed in the holding mechanism, as discussed in Section 2. To confirm the effect of the elongation rate α_m on wheel slippage and vertical vibration, two types of urethane rubber block, one with a Shore A hardness of 50 and the other a Shore A hardness of 70, both with dimensions of $4\text{mm} \times 10\text{mm} \times 15\ \text{mm}$, are used in prototype A. The prototype vehicles with these rubber blocks are referred to as prototype A-50 and prototype A-70, respectively.

For prototype B, the left wheel is the AOWBR and the right wheel is a conventional omni wheel. These wheels have the same shape and are coaxially arranged, as shown in Fig. 13. The AOWBR has a single row of barrel-shaped outer rollers around its circumference (total of eight rollers). The setting angle between the transmission roller and the outer roller γ is $90°$. To realize the condition $\gamma = 90°$, some gaps are provided to avoid interference between the outer rollers. Urethane rubber with a Shore A hardness of 50 is used in the holding mechanism for this prototype vehicle.

To make the comparison between the two types of prototype as fair as possible, the total mass of each prototype was adjusted to 96.5 kg. All experiments were conducted without a passenger on board. The same motors (Maxon RE65 250 W) were used to

drive the wheels of both prototypes. The control system in each prototype was composed of a microcomputer (Arduino Mega or Arduino Micro) and motor drivers (Maxon ESCON).

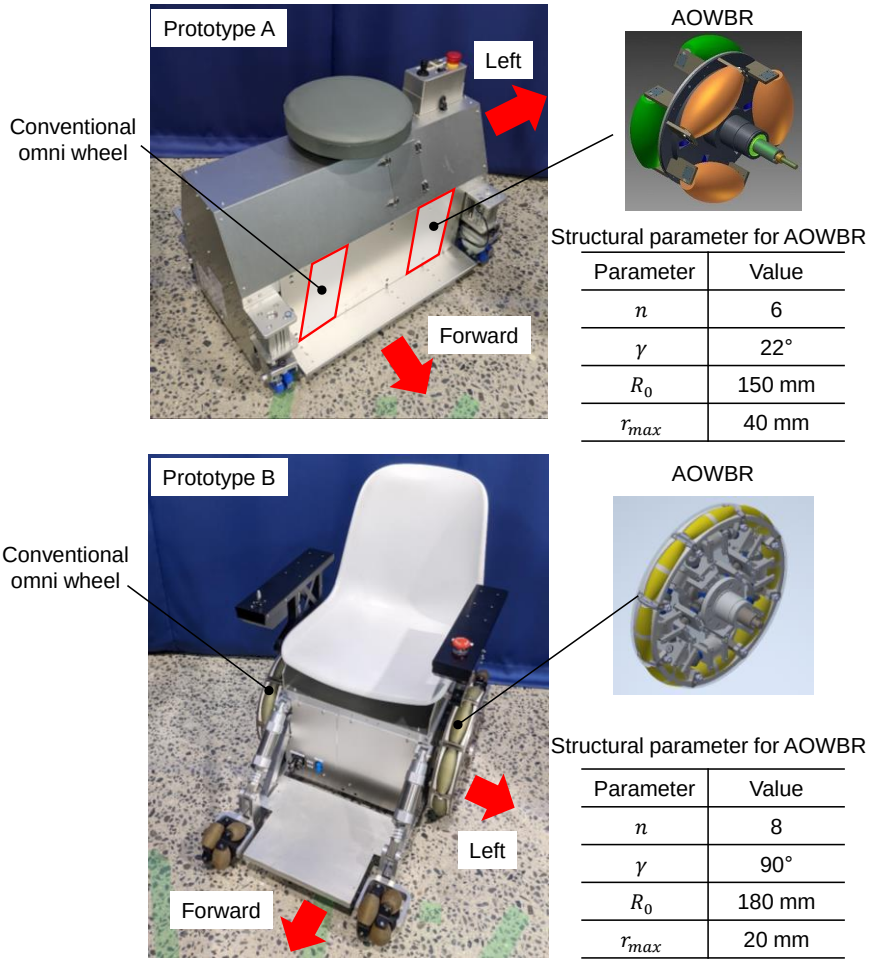

Parameter	Value
n	6
γ	22°
R_0	150 mm
r_{max}	40 mm

Parameter	Value
n	8
γ	90°
R_0	180 mm
r_{max}	20 mm

Fig. 13 Prototype vehicles with one AOWBR and one conventional omni wheel.

4.2 Slippage experiments and results

Experiments were conducted to confirm the effect of the design parameters on wheel slippage. Both vehicles were commanded to move toward the left at a velocity of $V = 0.5\ \mathrm{km/h}$. The AOWBR was set to contact the ground at the r_{max} section of the outer roller when the vehicles started to move. This experiment was conducted five

times for each type of vehicle. The trajectory of the vehicles was recorded by a three-dimensional motion capture system (Vicon MX Bonita 3 and 10, Vicon Motion Systems Ltd.), which was used to calculate the actual distance traveled by the vehicles. The accuracy of Vicon is sub-millimeter, which depends on the distance from the camera to the marker.

The slip rate was used to evaluate wheel slippage. It is defined as:

$$S = \frac{L_t - L_a}{L_t} \times 100\%, \tag{9}$$

where L_a and L_t are respectively the actual and theoretical travel distances of the prototype vehicle. Here, L_a can be obtained from the three-dimensional motion capture system and L_t is calculated as:

$$L_t = \frac{2\pi r_{max}}{n_1 n_2} \omega_d, \tag{10}$$

where n_1 is the reduction ratio between the motor and the output shaft of the AOWBR, n_2 is the reduction ratio between the output shaft and the outer roller, and ω_d is the rotational velocity of the motor. The rotational velocity of the motor is measured by a rotary encoder mounted on the motor (HEDL 5540, Maxon Motor AG). The resolution of the rotary encoder is 500 counts per revolution.

First, the actual trajectories of the prototype vehicle are compared with the trajectory calculated from the motor rotations recorded by the rotary encoder. As shown in Fig. 14, the longitudinal position is almost always zero. Specifically, the longitudinal error is smaller than 4 mm even when the vehicle moves about 1200 mm in the left direction. On the other hand, the actual moving distance along the left direction

of each prototype vehicle is smaller than the calculated one, which means that the slippage occurs.

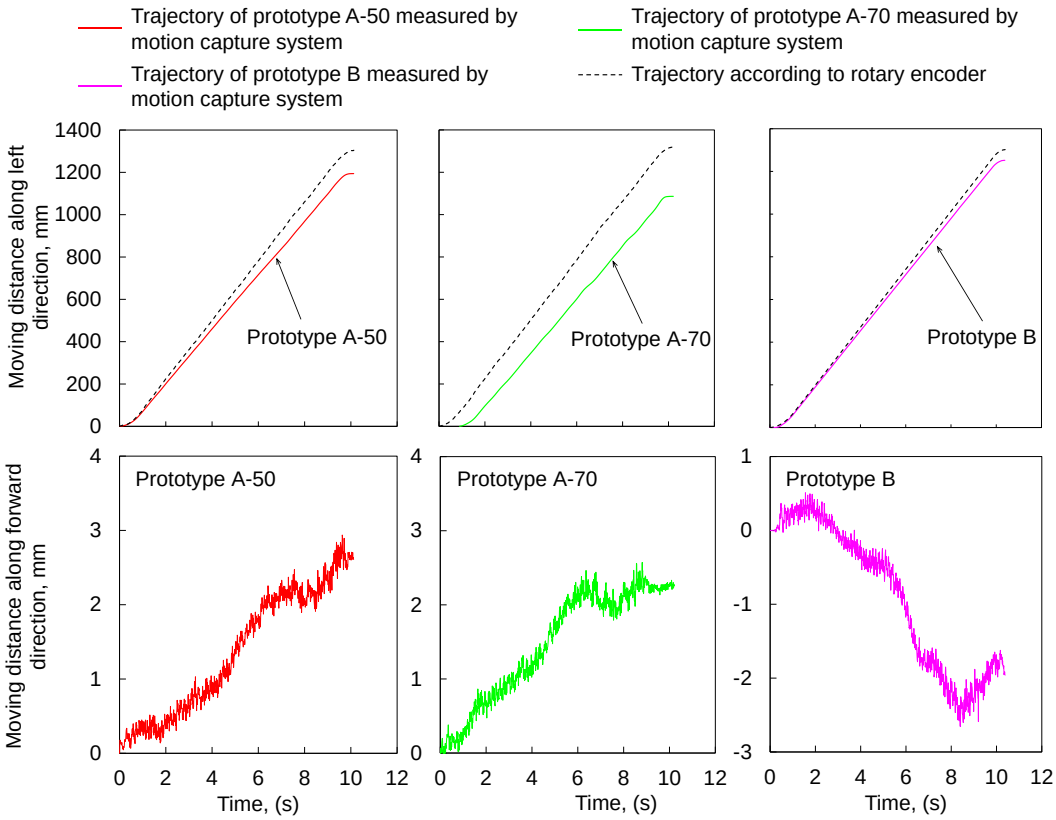

Fig. 14 Comparison of trajectories measured by motion capture system and that calculated from rotary encoder

To evaluate the slip situation of each prototype vehicle, the slip rate is discussed. The slip rate of each vehicle in each experiment is summarized in Fig. 15, where the symbols represent the slip rate in each trial, and the color bars (annotations are the exact values) show the average slip rate. The confidence interval at a 5% significance level is indicated by the error bar. The p-values obtained using Welch's t-test are also shown in the figure. The slip rate for prototype A-50 is much smaller than that of prototype A-70. The difference in average values shows a 1% significance level ($p < 0.01$). This indicates that

a harder rubber block leads to more slippage, which agrees with the simulation results shown in Fig. 9.

Compared with the slip rate for prototype A-50, that for prototype B is smaller ($p <$ 0.05) even though these vehicles had the same hardness of the rubber block. The difference is statistically significant at a level of 5% ($p < 0.05$). Here, the ground contact point did not change in the circumferential direction of the main wheel, so the effect of the number of outer rollers is considered to be small. The main reason for the difference in the slip rate is thus thought to be the setting angle between the transmission roller and outer roller. The setting angle for prototype B is larger than that for prototype A-50. This verifies that a larger setting angle increases the pressing force between the transmission roller and outer roller, as shown in the simulation (Fig. 10). The difference between the average slip rates of prototype A-70 and prototype B is statistically significant at a level of 1% ($p < 0.01$). Additionally, in terms of slip rate, the difference between prototype B and prototype A-70 is larger than that between prototype A-50 and prototype A-70. This indicates that selecting a larger setting angle is more beneficial for reducing wheel slippage than changing the hardness of the rubber block.

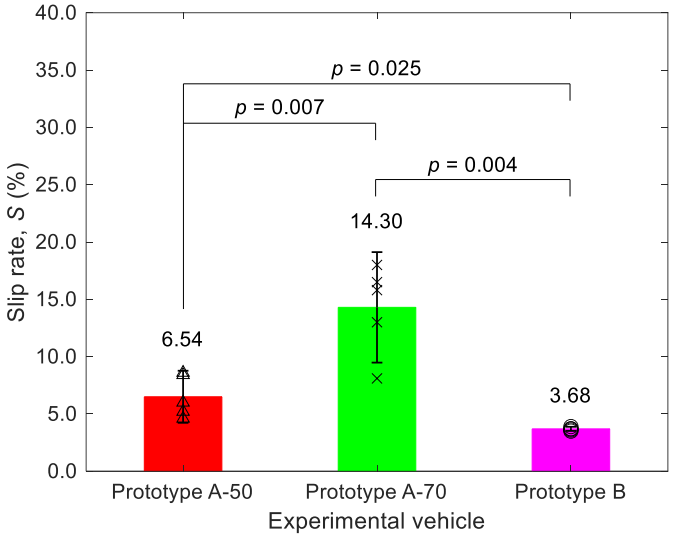

Fig. 15 Slip rate for prototype vehicles during movement.

4.3 Vibration experiments and results

To evaluate the effect of the design parameters on vibration during movement, the vertical vibration of the vehicles was measured during forward movement. The velocity was set to $V = 1\ \mathrm{km/h}$. An acceleration meter (Sorocaba-1, Cosmic ME Co., Inc.) with a MEMS-type sensor tip (LIS344ALH, STMicroelectronics), which was fixed at the center of the top plane of the vehicles after the seats were removed, was used to measure the acceleration in the vertical direction. The sensitivity of the acceleration meter is 98.8% for 9.8 m/s^2. The sampling range was 20 m/s^2 and the sampling frequency was 1000 Hz. A median filter with a size of 0.01 s was applied to remove noise from the measured vertical vibration.

The calculation results for the frequency analysis are shown in Fig. 16. The vertical dotted lines in the figure indicate multiples of the specific frequency f of the vibration caused by switching of the outer rollers. This frequency can be calculated as:

$$f = \frac{V}{2\pi R_0} n. \tag{10}$$

The specific frequency f for prototype A and prototype B, 1.77 and 1.97 Hz, respectively, was obtained using the parameters shown in Fig. 13. The recommended amplitude limit proposed by Janeway [32] was used to evaluate the vibration strength, which is shown by the blue dash-dotted line in the figure. When the amplitude exceeds the limit, the passenger may feel discomfort. As shown in Fig. 16, the vibration of prototypes A-50 and A-70 is always below the limit, whereas that of prototype B has some peaks beyond or close to the limit at several frequencies, namely multiples of the switching frequency of the outer rollers (i.e., f, $2f$, $3f$, and so on). These peaks are considered to be generated mainly by the gaps between the outer rollers. Except for these peak vibrations, there is no obvious difference among the magnitude and distribution of the vibration of these prototypes. It is inferred that the structural parameters for the AOWBR have only a slight effect on the vehicle vibration.

A close observation of the vibration of prototypes A-50 and A-70 indicates that some peaks also appear at multiples of the switching frequency of the outer rollers, as shown in Fig. 16(a). Vibration at these frequencies might be caused partly by the displacement of the outer rollers when they contact the ground. For example, in the simulation, z_t caused vibration at frequency f. On the other hand, the effect of the hardness of the rubber block on vibration seems limited, as inferred from a comparison of the results for prototypes A-50 and A-70. Therefore, the vibration caused by resonance might be dominant. Based on this result, more attention should be paid to avoiding resonance rather than the vibration strength dependent on the design parameters of the AOWBR.

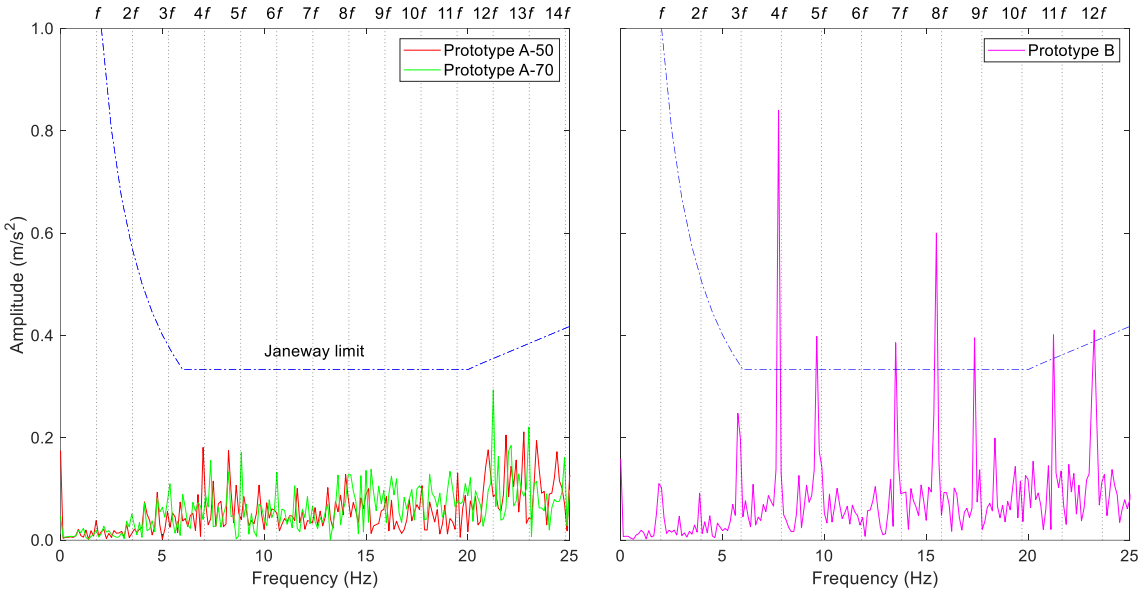

(a) (b)

Fig. 16 Frequency analysis results for vertical vibration during vehicle movement for (a) prototype A (f = 1.77 Hz) and (b) prototype B (f = 1.97 Hz).

The simulation and experiment results are summarized in Table 2. Both simulation and experiment show similar results that a larger setting angle and a softer rubber block are effective in suppressing roller slippage in the design of the AOWBR. The vibration due to the displacement of the outer rollers has a limited influence on vehicle vibration. Since the total number of the outer rollers hardly affects the vertical vibration and wheel slippage directly, it should be determined by considering the number of parts and avoidance of resonance with the vehicle body. Then, the radius of the outer rollers can be determined properly to get close to the above design purpose.

Table 2 Comparison of simulation and experiment results

		Harder rubber block	Larger setting angle of outer roller	Smaller radius of outer roller	Larger number of outer rollers
Simulation	Pressing force N_d	Negative	Positive	Little correlation	Little correlation
	Vertical displacement z_1	Negative	Negative	Little correlation	Little correlation
Experiment	Non-slippage	Negative	Positive		
	Vibration	Little correlation	Little correlation		

5. CONCLUSION

The AOWBR was previously proposed to meet the requirements of omnidirectional mobility and small vibration. A friction drive is used to drive the outer roller to realize lateral movement. However, slippage may occur between an outer roller and the corresponding transmission roller, which would lead to errors in the motion control of a vehicle equipped with the AOWBR. To solve this problem, this study investigated the relationship between the structural parameters and wheel slippage and vibration. The following results were obtained:

1) Under the assumption of no slippage between the wheel and the ground, the kinetic model for the whole AOWBR was separated into those for the wheel main body, the transmission roller, and the outer roller.
2) Based on the kinetic models, simulations were conducted to examine the dynamic characteristics of the AOWBR. The results show that the pressing force between the transmission and outer rollers, and the vertical displacement of the main wheel increase when the hardness of the rubber block in the holding mechanism is softer.

Additionally, when the setting angle between the transmission and outer rollers is increased, the pressing force increases whereas the vertical displacement decreases. The total number of outer rollers and the maximum cross-sectional radius of the outer roller have little influence on the pressing force and vertical displacement. It is inferred that softer rubber and a larger setting angle contributed to reducing wheel slippage and vibration. The AOWBR has high design freedom in terms of the total number of outer rollers and the radius of the outer roller for avoiding wheel slippage and vibration.

3) Experiments were conducted to measure slippage and vibration using two types of prototype vehicle. The experimental results show that a softer rubber block and a larger setting angle lead to less slippage, which agrees with the simulation results. It also shows that the variation of the vehicle vibration calculated in the simulation is small on the scale of the practical vehicle, and the difference in the structural parameters of the AOWBR does not cause unacceptable vibration.

This study mainly focused on the motion characteristics of the AOWBR when it moved forward. On the other hand, the motion characteristics may be changed when it turns on the spot maneuvers because of the effect of the centrifugal force and self-aligning torque. This will be investigated in the future.

ACKNOWLEDGMENT

This work was supported by JSPS KAKENHI grant number JP21K14067, JP25289023. We would like to thank Mr. Sakamoto and the employees of Issi Corporation for their

cooperation. We thank Mr. Yamaguchi and the members of mechanism and motion engineering laboratory of Kyoto university for their support.

NOMENCLATURE

A	Cross-sectional area of rubber block
b	Correction term
C_{rr}	Resistance coefficient
F_{2ax}, F_{2bx},	Forces from transmission roller at each end along positive X_2-axis
F_{2ay}, F_{2by},	Forces from transmission roller at each end along positive Y_2-axis
F_{2az}, F_{2bz}	Forces from transmission roller at each end along positive Z_2-axis
F_{3ax}, F_{3bx}	Forces from outer roller at each end along positive X_3-axis
F_{3ay}, F_{3by}	Forces from outer roller at each end along positive Y_3-axis
F_{3az}, F_{3bz}	Forces from outer roller at each end along positive Z_3-axis
f	Driving force
I	Inertia moment of wheel main body around X_1-axis
I_3	Inertia moment of outer roller around X_3-axis
K_t	Parameter that depends on dicumyl peroxide content in rubber
k_1	Modulus of elasticity between transmission roller and outer roller
L_2	Distance from center point of transmission roller to its support point

L_3	Distance from center point of outer roller to holding mechanism
L_a	Actual travel distance of prototype vehicle
L_t	Theoretical travel distance of prototype vehicle
l	Original length of rubber block
l_2	Distance from center point of wheel main body to that of transmission roller
m_i $(i = 1, 2, 3)$	Mass of wheel main body, transmission roller, and outer roller
N	Normal force from wheel to ground
N_d	Pressing force from outer roller to transmission roller
n	Total number of outer rollers
n_1	Reduction ratio between motor and output shaft
n_2	Reduction ratio between output shaft and outer roller
p	Significance probability
R_0	Radius of main wheel without consideration of deformation of outer roller
r_{max}	Maximum radius of cross section of outer roller
r_d	Radius of the transmission roller
S	Slip rate
V	Moving velocity

x_1, y_1, z_1	Displacement of wheel main body along X_1-, Y_1-, Z_1-axes direction
x_2, y_2, z_2	Displacement of transmission roller along X_2-, Y_2-, Z_2-axes direction
x_3, y_3, z_3	Deformation of outer roller along X_3-, Y_3-, Z_3-axes direction
α_l, α_r	Elongation rate for rubber block in holding mechanism at left and right sides, respectively
α_m	Maximum elongation rate for rubber
γ	Setting angle between transmission roller and outer roller
θ_1	Rotation angle of wheel main body around X_1-axis
θ_3	Rotation angle of outer roller around X_3-axis
τ_1	Driving torque carried on wheel main body
ω_d	Rotational velocity of motor

REFERENCES

[1] Siegwart, R., Nourbakhsh, I. R., & Scaramuzza, D., 2011, Introduction to autonomous mobile robots. MIT press, Cambridge, USA, Chap. 2, ISBN: 978-0-26-201535-6.

[2] Taheri, H., & Zhao, C. X., 2020, "Omnidirectional mobile robots, mechanisms and navigation approaches," Mechanism and Machine Theory, vol. 153, 103958. doi: 10.1016/j.mechmachtheory.2020.103958.

[3] Yu , H., Spenko , M., and Dubowsky, S., 2004, "Omni-Directional Mobility Using Active Split Offset Castors ." ASME. J. Mech. Des., vol. 126, no. 5, pp. 822–829. doi: 10.1115/1.1767181.

[4] Takane, E., Tadakuma, K., Watanabe, M., Konyo, M., and Tadokoro, S., 2021, "Design and Control Method of a Planar Omnidirectional Crawler Mechanism." ASME. J. Mech. Des., vol. 144, no. 1: 013302. https://doi.org/10.1115/1.4051354

[5] Indiveri, G., 2009, "Swedish Wheeled Omnidirectional Mobile Robots: Kinematics Analysis and Control," IEEE Transactions on Robotics, vol. 25, no. 1, pp. 164-171. doi: 10.1109/TRO.2008.2010360.

[6] Bi, Z. M., Wang, L., 2010, "Dynamic control model of a cobot with three omni-wheels," Robotics and Computer-Integrated Manufacturing, vol. 26, no. 6, pp. 558-563. doi: 10.1016/j.rcim.2010.06.022.

[7] Hijikata, M, Miyagusuku R, Ozaki K., 2022, "Wheel Arrangement of Four Omni Wheel Mobile Robot for Compactness," Applied Sciences. vol. 12, no. 12, 5798. doi: 10.3390/app12125798

[8] Kim, C., Suh, J., & Han, J. H., 2020, "Development of a hybrid path planning algorithm and a bio-inspired control for an omni-wheel mobile robot," Sensors, vol. 20, no. 15, 4258. doi: 10.3390/s20154258

[9] Şahin, O., & Dede, M., 2021, "Investigation of longitudinal friction characteristics of an omnidirectional wheel via LuGre model," Robotica, vol. 39, no. 9, pp. 1654-1673. doi:10.1017/S0263574720001423.

[10] Weiss, A., Langlois, R. G., and Hayes, M. J. D., 2011, "Unified Treatment of the Kinematic Interface Between a Sphere and Omnidirectional Wheel Actuators." ASME. J. Mechanisms Robotics; vol. 3, no. 4: 041001. doi: 10.1115/1.4004888.

[11] Gfrerrer, A., 2008, "Geometry and kinematics of the Mecanum wheel," Computer Aided Geometric Design, vol. 25, no. 9, pp. 784-791. doi: 10.1016/j.cagd.2008.07.008.

[12] Zhang, D., Wang, G. and Wu, Z., 2022, "Reinforcement Learning-Based Tracking Control for a Three Mecanum Wheeled Mobile Robot," IEEE Transactions on Neural Networks and Learning Systems, pp. 1-8. doi: 10.1109/TNNLS.2022.3185055.

[13] Cao, G., Zhao, X., Ye, C. et al., 2022, "Fuzzy adaptive PID control method for multi-mecanum-wheeled mobile robot," Journal of Mechanical Science and Technology, vol. 36, pp. 2019–2029. doi: 10.1007/s12206-022-0337-x.

[14] Ye, C., Zhang, J., Yu, S. and Ding, G., 2019, "Movement Performance Analysis of Mecanum Wheeled Omnidirectional Mobile Robot," 2019 IEEE International Conference on Mechatronics and Automation (ICMA), pp. 1453-1458. doi: 10.1109/ICMA.2019.8816397.

[15] Granados, E. Boularias, A. Bekris, K. and Aanjaneya, M., 2022, "Model Identification and Control of a Low-cost Mobile Robot with Omnidirectional Wheels using Differentiable Physics," 2022 International Conference on Robotics and

Automation (ICRA), pp. 1358-1364. doi: 10.1109/ICRA46639.2022.9812454.

[16] Xiao, H., Yu, D., & Chen, C. P., 2022, "Self-triggered-organized mecanum-wheeled robots consensus system using model predictive based protocol," Information Sciences, 590, 45-59. doi: 10.1016/j.ins.2021.12.108.

[17] Wang, Y., Guan, X., Hu, T., Zhang, Z., Wang, Y. et al., 2021, "Fuzzy PID Controller Based on Yaw Angle Prediction of a Spherical Robot," 2021 IEEE/RSJ International Conference on Intelligent Robots and Systems (IROS), pp. 3242-3247. doi: 10.1109/IROS51168.2021.9636425.

[18] Zhang, Z., Wan, Y., Wang, Y., Guan, X., Ren, W., Li, G., 2021, "Improved hybrid A* path planning method for spherical mobile robot based on pendulum," International Journal of Advanced Robotic Systems. vol. 18, no. 1. doi: 10.1177/1729881421992958.

[19] Hu, Y., Wei, Y., and Liu, M., 2021, "Design and Performance Evaluation of a Spherical Robot Assisted by High-Speed Rotating Flywheels for Self-Stabilization and Obstacle Surmounting." ASME. J. Mechanisms Robotics; vol. 13, no. 6 : 061001. doi: 10.1115/1.4050623.

[20] Akella, P., O'Reilly, O. M., and Sreenath, K., 2019, "Controlling the Locomotion of Spherical Robots or Why BB-8 Works." ASME. J. Mechanisms Robotics; vol. 11, no. 2: 024501. doi: 10.1115/1.4042296.

[21] Tafrishi, S. A., Svinin, M., Esmaeilzadeh, E., and Yamamoto, M., 2019, "Design, Modeling, and Motion Analysis of a Novel Fluid Actuated Spherical Rolling Robot." ASME. J. Mechanisms Robotics, vol. 11, no. 4: 041010. doi: 10.1115/1.4043689.

[22] Gao, X., Yan, L., He, Z., Wang, G., and Chen, I., 2022, "Design and Modeling of a Dual-Ball Self-Balancing Robot," IEEE Robotics and Automation Letters, vol. 7, no. 4, pp. 12491-12498. doi: 10.1109/LRA.2022.3219029.

[23] Komori, M., Matsuda, K., Terakawa, T., Takeoka, F., Nishihara, H., & Ohashi, H., 2016,"Active omni wheel capable of active motion in arbitrary direction and omnidirectional vehicle," Journal of Advanced Mechanical Design, Systems, and Manufacturing, vol. 10, no. 6, JAMDSM0086-JAMDSM0086. doi: 10.1299/jamdsm.2016jamdsm0086.

[24] Terakawa, T., Komori, M., Sakamoto, M., Kawato, Y., Morita, Y., & Nishida, Y., 2019, "Two-wheel-drive vehicle that is movable in the longitudinal and lateral directions with a small number of motors," Journal of Japan Society for Design Engineering, vol. 54, no. 2, pp. 145-160. doi: 10.14953/jjsde.2018.2811

[25] Komori, M., Matsuda, K., 2018, "Velocity Characteristics of Active Omni Wheel Considering Transmitting Mechanism, " European Conference on Mechanism Science, pp. 109-116. doi: 10.1007/978-3-319-98020-1_13.

[26] Terakawa, T., Komori, M., Yamaguchi, Y., & Nishida, Y., 2019, "Active omni wheel possessing seamless periphery and omnidirectional vehicle using it," Precision Engineering, vol. 56, pp. 466-475. doi: 10.1016/j.precisioneng.2019.02.003.

[27] Long, S., Terakawa, T., Komori, M., Nishida, Y., Ougino, T., & Hattori, Y., 2021, "Effect of double-row active omni wheel on stability of single-track vehicle in roll direction," Mechanism and Machine Theory, vol. 163, 104374. doi: 10.1016/j.mechmachtheory.2021.104374.

[28] Galati, R., Mantriota, G., & Reina, G., 2022, “Adaptive heading correction for an industrial heavy-duty omnidirectional robot,” Scientific Reports, vol. 12, 19608. doi: 10.1038/s41598-022-24270-x.

[29] Bae, J. J., & Kang, N., 2016), “Design optimization of a mecanum wheel to reduce vertical vibrations by the consideration of equivalent stiffness,” Shock and Vibration. doi: 10.1155/2016/5892784.

[30] Furukawa, J., Okamoto, H., Inagaki, S., 1976, "Rubber Elasticity at large deformation (Ⅰ): theory of stress-strain behavior of vulcanized rubber at large deformation," Nippon Gomu Kyokaishi, vol. 49, no. 7, pp. 596-601. doi: 10.2324/gomu.49.7_596. (In Japanese)

[31] Okamoto, H., Furukawa, J., Inagaki, S., 1976, "Rubber elasticity at large deformation (Ⅱ): stress-strain behavior of natural rubber vulcanizates," Nippon Gomu Kyokaishi, vol. 49, no. 8, pp. 620-627 (In Japanese). doi: 10.2324/gomu.49.8_620.

[32] Janeway, R., 1975, "Human Vibration Tolerance Criteria and Applications to Ride Evaluation," SAE Technical Paper, 750166. doi: 10.4271/750166.

Table Caption List

Table 1 Standard parameter values used in simulation (parameters on left side were fixed and parameters on right side were varied)

Table 2 Comparison of simulation and experiment results

Figure Captions List

Fig. 14 Comparison of trajectories measured by motion capture system and that calculated from rotary encoder

Fig. 15 Slip rate for prototype vehicles during movement

Fig. 16 Frequency analysis results for vertical vibration during vehicle movement for (a) prototype A (f = 1.77 Hz) and (b) prototype B (f = 1.97 Hz)